BELLE-CONF-0003
Parallel Session: PA-07
Plenary Session: PL-01b

Studies of Radiative B Meson Decays with Belle

The Belle Collaboration

Abstract

We have studied radiative B meson decays using a 5.1 fb^{-1} data sample collected at the $\Upsilon(4S)$ resonance with the Belle detector at the KEKB e^+e^- collider. The inclusive branching fraction $\mathcal{B}(b\to s\gamma) = (3.34 \pm 0.50^{+0.34+0.26}_{-0.37-0.28}) \times 10^{-4}$ is measured using a technique to subtract the background contribution that requires a relatively small amount of off-resonance data. We measure the exclusive branching fractions to the $K^*\gamma$ final states to be $\mathcal{B}(B^0\to K^*(892)^0\gamma) = (4.94 \pm 0.93^{+0.55}_{-0.52}) \times 10^{-5}$ and $\mathcal{B}(B^+\to K^*(892)^+\gamma) = (2.87 \pm 1.20^{+0.55}_{-0.40}) \times 10^{-5}$. We searched for $B \to \rho\gamma$ decays and obtained an upper limit of $\mathcal{B}(B \to \rho\gamma)/\mathcal{B}(B\to K^*\gamma) < 0.28$ (90% C.L.), where Belle's good high momentum kaon identification is used to reduce the contribution from $B\to K^*\gamma$ to a negligible level.

Typeset using REVTEX

A. Abashian[44], K. Abe[8], K. Abe[36], I. Adachi[8], Byoung Sup Ahn[14], H. Aihara[37], M. Akatsu[19], G. Alimonti[7], K. Aoki[8], K. Asai[20], M. Asai[9], Y. Asano[42], T. Aso[41], V. Aulchenko[2], T. Aushev[12], A. M. Bakich[33], E. Banas[15], S. Behari[8], P. K. Behera[43], D. Beiline[2], A. Bondar[2], A. Bozek[15], T. E. Browder[7], B. C. K. Casey[7], P. Chang[23], Y. Chao[23], B. G. Cheon[32], S.-K. Choi[6], Y. Choi[32], Y. Doi[8], J. Dragic[17], A. Drutskoy[12], S. Eidelman[2], Y. Enari[19], R. Enomoto[8,10], C. W. Everton[17], F. Fang[7], H. Fujii[8], K. Fujimoto[19], Y. Fujita[8], C. Fukunaga[39], M. Fukushima[10], A. Garmash[2,8], A. Gordon[17], K. Gotow[44], H. Guler[7], R. Guo[21], J. Haba[8], T. Haji[4], H. Hamasaki[8], K. Hanagaki[29], F. Handa[36], K. Hara[27], T. Hara[27], T. Haruyama[8], N. C. Hastings[17], K. Hayashi[8], H. Hayashii[20], M. Hazumi[27], E. M. Heenan[17], Y. Higashi[8], Y. Higasino[19], I. Higuchi[36], T. Higuchi[37], T. Hirai[38], H. Hirano[40], M. Hirose[19], T. Hojo[27], Y. Hoshi[35], K. Hoshina[40], W.-S. Hou[23], S.-C. Hsu[23], H.-C. Huang[23], Y.-C. Huang[21], S. Ichizawa[38], Y. Igarashi[8], T. Iijima[8], H. Ikeda[8], K. Ikeda[20], K. Inami[19], Y. Inoue[26], A. Ishikawa[19], R. Itoh[8], G. Iwai[25], M. Iwai[8], H. Iwasaki[8], Y. Iwasaki[8], D. J. Jackson[27], P. Jalocha[15], H. K. Jang[31], M. Jones[7], R. Kagan[12], H. Kakuno[38], J. Kaneko[38], J. H. Kang[45], J. S. Kang[14], P. Kapusta[15], K. Kasami[8], N. Katayama[8], H. Kawai[3], M. Kawai[8], N. Kawamura[1], T. Kawasaki[25], H. Kichimi[8], D. W. Kim[32], Heejong Kim[45], H. J. Kim[45], Hyunwoo Kim[14], S. K. Kim[31], K. Kinoshita[5], S. Kobayashi[30], S. Koike[8], Y. Kondo[8], H. Konishi[40], K. Korotushenko[29], P. Krokovny[2], R. Kulasiri[5], S. Kumar[28], T. Kuniya[30], E. Kurihara[3], A. Kuzmin[2], Y.-J. Kwon[45], M. H. Lee[8], S. H. Lee[31], C. Leonidopoulos[29], H.-B. Li[11], R.-S. Lu[23], Y. Makida[8], A. Manabe[8], D. Marlow[29], T. Matsubara[37], T. Matsuda[8], S. Matsui[19], S. Matsumoto[4], T. Matsumoto[19], K. Misono[19], K. Miyabayashi[20], H. Miyake[27], H. Miyata[25], L. C. Moffitt[17], G. R. Moloney[17], G. F. Moorhead[17], N. Morgan[44], S. Mori[42], T. Mori[4], A. Murakami[30], T. Nagamine[36], Y. Nagasaka[18], Y. Nagashima[27], T. Nakadaira[37], T. Nakamura[38], E. Nakano[26], M. Nakao[8], H. Nakazawa[4], J. W. Nam[32], S. Narita[36], Z. Natkaniec[15], K. Neichi[35], S. Nishida[16], O. Nitoh[40], S. Noguchi[20], T. Nozaki[8], S. Ogawa[34], R. Ohkubo[8], T. Ohshima[19], Y. Ohshima[38], T. Okabe[19], T. Okazaki[20], S. Okuno[13], S. L. Olsen[7], W. Ostrowicz[15], H. Ozaki[8], P. Pakhlov[12], H. Palka[15], C. S. Park[31], C. W. Park[14], H. Park[14], L. S. Peak[33], M. Peters[7], L. E. Piilonen[44], E. Prebys[29], J. Raaf[5], J. L. Rodriguez[7], N. Root[2], M. Rozanska[15], K. Rybicki[15], J. Ryuko[27], H. Sagawa[8], Y. Sakai[8], H. Sakamoto[16], H. Sakaue[26], M. Satapathy[43], N. Sato[8], A. Satpathy[8,5], S. Schrenk[44], S. Semenov[12], Y. Settai[4], M. E. Sevior[17], H. Shibuya[34], B. Shwartz[2], A. Sidorov[2], V. Sidorov[2], S. Stanič[42], A. Sugi[19], A. Sugiyama[19], K. Sumisawa[27], T. Sumiyoshi[8], J. Suzuki[8], J.-I. Suzuki[8], K. Suzuki[3], S. Suzuki[19], S. Y. Suzuki[8], S. K. Swain[7], H. Tajima[37], T. Takahashi[26], F. Takasaki[8], M. Takita[27], K. Tamai[8], N. Tamura[25], J. Tanaka[37], M. Tanaka[8], Y. Tanaka[18], G. N. Taylor[17], Y. Teramoto[26], M. Tomoto[19], T. Tomura[37], S. N. Tovey[17], K. Trabelsi[7], T. Tsuboyama[8], Y. Tsujita[42], T. Tsukamoto[8], T. Tsukamoto[30], S. Uehara[8], K. Ueno[23], N. Ujiie[8], Y. Unno[3], S. Uno[8], Y. Ushiroda[16], Y. Usov[2], S. E. Vahsen[29], G. Varner[7], K. E. Varvell[33], C. C. Wang[23], C. H. Wang[22], M.-Z. Wang[23], T.-J. Wang[11], Y. Watanabe[38], E. Won[31], B. D. Yabsley[8], Y. Yamada[8], M. Yamaga[36], A. Yamaguchi[36], H. Yamaguchi[8], H. Yamamoto[7], H. Yamaoka[8], Y. Yamaoka[8], Y. Yamashita[24], M. Yamauchi[8], S. Yanaka[38], M. Yokoyama[37], K. Yoshida[19], Y. Yusa[36], H. Yuta[1], C.-C. Zhang[11], H. W. Zhao[8], Y. Zheng[7], V. Zhilich[2], and D. Žontar[42]

[1]Aomori University, Aomori

[2]Budker Institute of Nuclear Physics, Novosibirsk
[3]Chiba University, Chiba
[4]Chuo University, Tokyo
[5]University of Cincinnati, Cincinnati, OH
[6]Gyeongsang National University, Chinju
[7]University of Hawaii, Honolulu HI
[8]High Energy Accelerator Research Organization (KEK), Tsukuba
[9]Hiroshima Institute of Technology, Hiroshima
[10]Institute for Cosmic Ray Research, University of Tokyo, Tokyo
[11]Institute of High Energy Physics, Chinese Academy of Sciences, Beijing
[12]Institute for Theoretical and Experimental Physics, Moscow
[13]Kanagawa University, Yokohama
[14]Korea University, Seoul
[15]H. Niewodniczanski Institute of Nuclear Physics, Krakow
[16]Kyoto University, Kyoto
[17]University of Melbourne, Victoria
[18]Nagasaki Institute of Applied Science, Nagasaki
[19]Nagoya University, Nagoya
[20]Nara Women's University, Nara
[21]National Kaohsiung Normal University, Kaohsiung
[22]National Lien-Ho Institute of Technology, Miao Li
[23]National Taiwan University, Taipei
[24]Nihon Dental College, Niigata
[25]Niigata University, Niigata
[26]Osaka City University, Osaka
[27]Osaka University, Osaka
[28]Panjab University, Chandigarh
[29]Princeton University, Princeton NJ
[30]Saga University, Saga
[31]Seoul National University, Seoul
[32]Sungkyunkwan University, Suwon
[33]University of Sydney, Sydney NSW
[34]Toho University, Funabashi
[35]Tohoku Gakuin University, Tagajo
[36]Tohoku University, Sendai
[37]University of Tokyo, Tokyo
[38]Tokyo Institute of Technology, Tokyo
[39]Tokyo Metropolitan University, Tokyo
[40]Tokyo University of Agriculture and Technology, Tokyo
[41]Toyama National College of Maritime Technology, Toyama
[42]University of Tsukuba, Tsukuba
[43]Utkal University, Bhubaneswer
[44]Virginia Polytechnic Institute and State University, Blacksburg VA
[45]Yonsei University, Seoul

I. INTRODUCTION

In the Standard Model (SM), radiative B meson decays ($b\to s(,d)\gamma$) dominantly proceed through an electroweak penguin diagram, and their branching fractions are calculated up to the next-to-leading order correction [1]. In principle, non-SM particles can be the virtual particle in the diagram's loop, making the branching fraction sensitive to new physics predictions. Experimental results [2] [3] on $\mathcal{B}(b\to s\gamma)$ have been obtained with model dependent uncertainties, but they already provide stringent limits on charged Higgs or SUSY particles [4]. Experimentally the exclusive branching fraction measurements are complementary, with no model dependence and smaller systematic uncertainties in the results.

Naively, the $b\to d\gamma$ process is suppressed relative to $b\to s\gamma$ by a factor of $|V_{td}/V_{ts}|^2$, and thus, is expected to be 14 to 60 times smaller [5]. The observation of this decay channel might provide a precise measurement of $|V_{td}/V_{ts}|$, the first direct CP violation measurement within the SM framework, and may relatively enhance the sensitivity to non-SM couplings that uncovers or constrains new physics [5]. Experimentally, the exclusive channel $B\to\rho\gamma$ can be distinguished from the $B\to K^*\gamma$ background using particle identification devices, even if the branching fraction is suppressed by more than a factor of 14.

We have analyzed a data sample of 5.3×10^6 $B\bar{B}$ events corresponding to an integrated luminosity of 5.1 fb^{-1} collected at the $\Upsilon(4S)$ resonance with the Belle detector at the KEKB e^+e^- collider [6]. For background estimations we analyzed a 0.6 fb^{-1} data sample taken 60 MeV below the resonance. The beam energies at the $\Upsilon(4S)$ resonance are approximately 3.5 GeV for positrons and 8.0 GeV for electrons.

A full description of the Belle detector is given in [7] and here we briefly describe the apparatus relevant for this analysis. Charged tracks are reconstructed inside a 1.5 T superconducting solenoid magnet with a 50 layer central drift chamber (CDC) [8], that covers 17° to 150° in the lab frame and is segmented into 5 axial and 4 stereo super layers. Tracks are then refitted with the CDC and a three layer double sided silicon vertex detector (SVD) [9]. For particle identification, we combine information from three detectors. The high momentum range, typically from 1 to 3.5 GeV/c, is covered by a silica aerogel cherenkov counter (ACC) [10], providing threshold type pion/kaon separation. The momentum range below 1.5 GeV/c is covered by a time-of-flight (TOF) [11] counter with 100 ps time resolution. The very low and high momentum ranges are covered with dE/dx information from CDC. Outside of the tracking and particle identification devices and inside the solenoid is an electromagnetic calorimeter (ECL) [12] that covers the entire tracking acceptance (17° to 150°) with 8736 CsI(Tl) crystals of 16.2 X_0 depth. The energy resolution for a 2.5 GeV photon is better than 2%.

II. INCLUSIVE ANALYSIS

We select events that contain a high energy (2.1 to 3.4 GeV in the $\Upsilon(4S)$ rest frame) photon (γ) candidate inside the acceptance of the barrel calorimeter ($33^\circ<\theta_\gamma<128^\circ$). The photon candidate is required to be consistent with an isolated electromagnetic shower, i.e., 95% of energy is within a 3×3 cell around the local energy maximum and there is no associated charged track. We combine it with photon clusters in the event and reject if the invariant mass is consistent with π^0 or η.

All charged particle tracks of good quality are selected to be both charged pion and kaon candidates. A kaon probability is formed from likelihood ratio variables that are individually calculated for ACC, TOF and CDC dE/dx. We apply a very loose requirement that the kaon probability is greater than 0.1 for kaon candidates and less than 0.9 for pion candidates; these retain 88% of kaons and 96% of pions. Neutral pion candidates are reconstructed from two photon clusters each with more than 50 MeV energy deposit, and required to be within 2σ of M_{π^0}. The π^0 momentum is refitted with a mass constraint. K^0_S candidates are reconstructed from two charged tracks, whose invariant mass is within 3σ of $M_{K^0_S}$. We require the K^0_S candidate to form a displaced vertex from the interaction point and in a direction consistent with the K^0_S momentum.

The inclusive reconstruction is performed by summing up multiple exclusive final states. We reconstruct strange final state X_s candidates that include one charged kaon or K^0_S and up to 4 pions of which no more than one is a π^0 (16 different combinations). We tested this method using a Monte Carlo simulation that consists of a $K^*(892)\gamma$ exclusive decay sample and an inclusive $b\to s\gamma$ decay sample for $M_{X_s} > 1.1$ GeV/c^2 that follows the mass spectrum of a spectator model [13] [14] and is hadronized with the JETSET [15] program. We found around 60% of events fall into one of the reconstructed combinations while the remaining events have either more than one kaon or more than one π^0 or other neutral particles (η, ϕ and K_L).

From the X_s and photon candidates, we form two independent kinematic variables, the beam constrained mass $M_B = \sqrt{E^2_{beam} - |\vec{p}_{X_s} + \vec{p}_\gamma|^2}$ and the energy difference $\Delta E = E_{X_s} + E_\gamma - E_{beam}$ in the $\Upsilon(4S)$ rest frame. E_{beam} is defined as the beam energy in the $\Upsilon(4S)$ rest frame. First, we select candidates in a loose window of $|\Delta E| < 0.15$ GeV and $M_B > 5.2$ GeV/c^2 and we require the X_s direction to be within 14° from the photon axis. In the case of multiple candidates, we select the best candidate that has a minimum absolute value of ΔE, and then apply a cut on M_B. The reason for selecting the best candidate with only one variable is to leave other variables for background suppression, since our final result is not limited by the signal reconstruction efficiency.

The dominant hard photon backgrounds come from the $e^+e^-\to q\bar{q}\gamma$ initial state radiation process and photons from the continuum $e^+e^-\to q\bar{q}$ process followed by neutral hadron decays ($\pi^0, \eta, \ldots$). In the $\pi^0 \to \gamma\gamma$ decay, the photons are either isolated in two calorimeter clusters or merged into one cluster. We optimize the cuts to maximize the signal significance $S/\sqrt{S+B}$ where S and B are the expected number of signal and background events, respectively. We determine the cut values of $M_B > 5272$ MeV/c^2 and $-100 < \Delta E < 80$ MeV. Combinatoric backgrounds from continuum events are further rejected using a new empirical event shape variable that we find to be more powerful than several existing variables such as the thrust angle, the normalized Fox-Wolfram parameters and the virtual calorimeter [16]. As in the other variables, the topology difference between spherical $B\bar{B}$ events and jet-like continuum events is exploited, using the relation between the B candidate axis and remaining tracks and topology among remaining tracks. We define the following eight variables

$$R^{maj}_l = \frac{\sum_i |p_i||p_\gamma| P_l(\cos\theta_{i\gamma})}{\sum_i |p_i||p_\gamma|}, \quad R^{min}_l = \frac{\sum_{i,j} |p_i||p_j| P_l(\cos\theta_{ij})}{\sum_{i,j} |p_i||p_j|}$$

where l runs from 1 to 4 for the Legendre function P_l and i, j run over all the neutral and

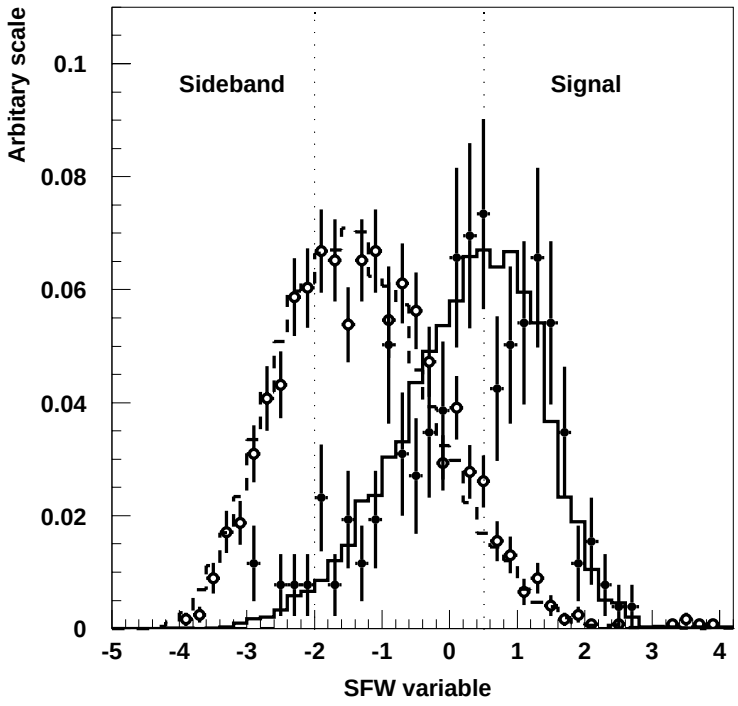

FIG. 1. The SFW variable distribution as described in text. The background distribution of off-resonance data (open circles) and the Monte Carlo expectation (dashed histogram) are shown. The signal distribution of $B \to D\pi$ data (solid circles) and signal Monte Carlo (solid histogram) are compared.

charged tracks that are not used to form the B candidate. Then we combine them into a Fisher discriminant [16]

$$\mathcal{F} = \sum_{l=1,4} \alpha_l R_l^{maj} + \sum_{l=1,4} \beta_l R_l^{min}$$

where the eight coefficients α_i and β_i are optimized to maximize the discrimination to 2.3σ separation, as shown in Fig. 1. We call this the *Super Fox-Wolfram* (SFW) variable, since the terms are combined in such a way to enhance the discrimination of the original definition of the Fox-Wolfram moments [17]. We select the events with $\mathcal{F} > 0.5$, which optimizes the significance and the systematic uncertainties.

We extract the signal yield from the photon energy spectrum. The background contribution is subtracted using events from a SFW sideband region ($\mathcal{F} < -2$), where only 2% of signal remains. Very little correlation between the photon candidate energy and the SFW variable is found either with the off-resonance data or a simulation study. The absolute scale is determined from the off-resonance data ratio between the signal and sideband region. In order to increase statistics, we relax the cuts to $|\Delta E| < 0.15$ GeV and $M_B > 5.22$ GeV/c^2

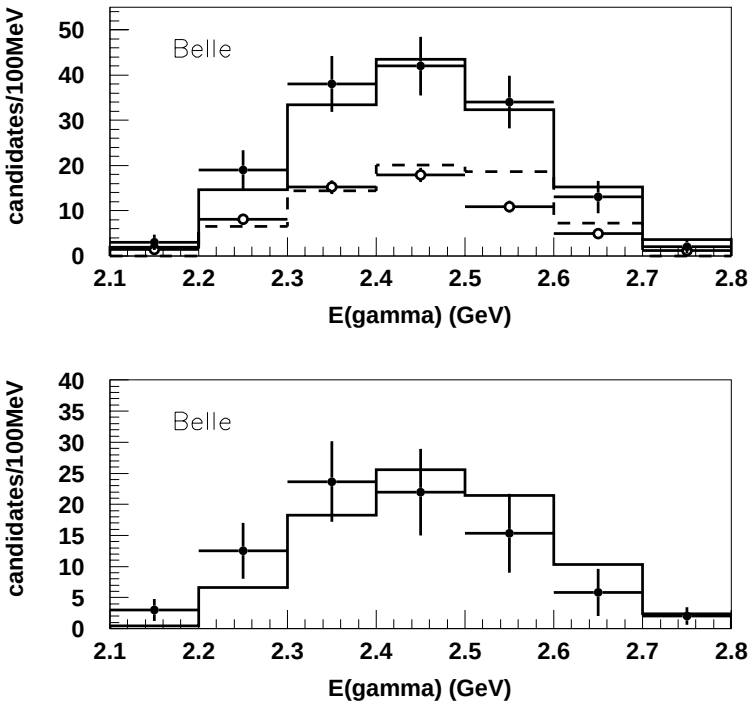

FIG. 2. The energy spectrum of photon candidates in the inclusive $b \to s\gamma$ analysis before (top) and after (bottom) background subtraction. The data points (solid circles) are compared with signal Monte Carlo (solid histogram). The background contribution (open circles) is estimated from the SFW sideband data as described in text and compared with continuum Monte Carlo (dashed histogram).

and remove the π^0/η veto. We find that varying the ΔE and SFW cuts does not change the absolute scale. The X_s direction cut is tuned to remove the correlation between M_B and the SFW variable, and we assign 6% uncertainty due to this correction.

Fig. 2 shows the photon energy spectrum for signal candidate events on top of the estimated background. We obtain 152 candidate events where 60.0 ± 6.5 background events are expected. This gives a signal yield of 92.0 ± 13.9 events. This background estimation method requires a relatively small amount of off-resonance data, and we have already obtained a statistical error of 15% with only 0.6 fb^{-1} of off-resonance data.

III. EXCLUSIVE ANALYSIS

The exclusive $B \to K^*\gamma$ analysis is performed by forming a B meson candidate with a photon candidate and a $K^*(892)$ candidate in the $K^+\pi^-$, $K^0_S\pi^0$, $K^0_S\pi^+$ or $K^+\pi^0$ channels (charge conjugated modes are implied). The photon, pion, kaon, π^0 and K^0_S selection criteria

are the same as used in the inclusive analysis. We require that the K^* invariant mass is within ± 75 MeV/c^2 of its nominal value. ΔE has an asymmetric distribution due to shower leakage and dead material in front of the calorimeter [12]. Therefore, we apply a cut of $-0.2 < \Delta E < 0.1$ GeV, keeping 90% of events. To calculate M_B, we constrain the photon energy so that $E_{beam} - E_{K^*} - E_\gamma = 0$. For the final states including π^0s, we constrain the energy of three photons together, including the photons from π^0 decay. With this procedure we improve the M_B resolution by about 20% to 2.8 MeV/c^2 (3.3 MeV/c^2) for the final states without (with) π^0. Although the M_B resolution is dominated by the contribution of the beam energy spread (0.07%), the π^0 energy resolution makes a significant contribution.

The $B \to \rho\gamma$ decay search is performed in a similar way, but in general with a tighter set of cuts to improve the expected $S/\sqrt{B}$ ratio. We tighten the kaon rejection condition and select tracks with kaon probability less than 0.4 as pion candidates; this retains 93% of pions and rejects 80% of kaons. We form $\rho(770)$ candidates in the $\pi^+\pi^-$ and $\pi^+\pi^0$ channels and require their invariant mass to be within ± 150 MeV/c^2 of M_ρ. We also reject events in the $B \to \rho(770)^0\gamma$ sample if the invariant mass falls within ± 50 MeV/c^2 of the nominal $K^*(892)^0$ mass when either of the charged pion is hypothesized to be a kaon. We select remaining events with $-100 < \Delta E < 80$ MeV. From a simulation study this procedure has about 50 times smaller efficiency for $K^*\gamma$ than for $\rho\gamma$ (see Fig. 3).

Continuum background is rejected with a likelihood ratio constructed from three variables; the SFW variable ($\mathcal{F}$), the B meson flight direction ($\cos\theta_B$) and the K^*/ρ decay helicity angle ($\cos\theta_H$). The likelihood ratio (LR) is defined as

$$LR = \frac{\mathcal{L}_s}{\mathcal{L}_s + \mathcal{L}_b}, \quad \mathcal{L}_{s,b} = p^F_{s,b}(\mathcal{F}) \times p^B_{s,b}(\cos\theta_B) \times p^H_{s,b}(\cos\theta_H)$$

where $p_s^{F,B,H}$ and $p_b^{F,B,H}$ are the probability density functions (PDF) for signal and background, respectively, for each of three variables. We obtained the PDFs from a Monte Carlo simulation. The signal PDFs are parametrized with an asymmetric Gaussian shape, $\sin^2\theta_B$ and $\sin^2\theta_H$. The first two parameters are common among exclusively reconstructed B decay channels while the last parameter characterizes the spin state. The background PDFs are parametrized with an asymmetric Gaussian shape for the SFW, a flat distribution for $\cos\theta_B$ and $a + \exp(b\cos\theta_H)$ for the helicity angle where a and b are given from a fit. We require the likelihood ratio to be greater than 0.7 for the $K^*\gamma$ analysis and 0.92 for the $\rho\gamma$ analysis, to accept 65% and 40% of the signals, respectively.

Then we extract the signal yield of $B \to K^*\gamma$ decays by fitting the M_B distribution with a Gaussian signal function and a threshold function for background. The fit is shown in Fig. 4. We obtain the signal shape from the $D\pi$ data and the background shape from the sideband data and fix them in the fitting. To obtain the uncertainty due to the fitting procedure, we vary the peak and width of the signal shape by 1σ and use background shapes from three different data samples. We count this uncertainty as the systematic error of the signal yield. Fig. 5 shows the ΔE distribution, which is in good agreement with our expectation.

For the $B \to \rho\gamma$ search, we find 0 and 3 events in the $\rho^0\gamma$ and $\rho^+\gamma$ signal windows, as shown in Fig. 6.

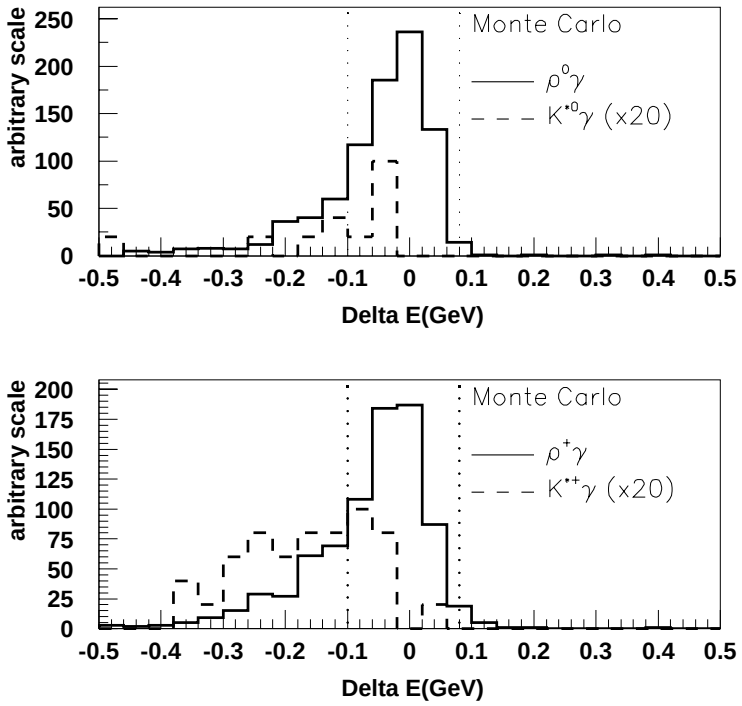

FIG. 3. The Monte Carlo ΔE distributions for the $B \to \rho(770)^0\gamma$ (top) and $B \to \rho(770)^+\gamma$ (bottom) channels. We compare the signal Monte Carlo (solid histogram) with the corresponding expected feedthrough from $B \to K^*\gamma$ (dashed histogram). Here we take into account the 20 times smaller branching fraction for $B \to \rho\gamma$. The dotted lines indicate the selected signal region.

IV. EXTRACTING RESULTS

The signal reconstruction efficiencies are tested with data. For every kind of final state particle, we select a different sample with large statistics. We compare the yield ratio between data and Monte Carlo to estimate how well our efficiencies are reproduced.

The high energy photon detection efficiency is checked with $e^+e^- \to e^+e^-\gamma$ events, where we can extract the expected photon energy and direction from e^+e^- momenta. The photon detection efficiency is calibrated with 5.3% uncertainty. We also nicely reproduce the asymmetric energy response of the calorimeter. The charged track reconstruction efficiency is tested with inclusive high momentum $\eta \to \pi^+\pi^-\pi^0$ and $\eta \to \gamma\gamma$ decays. We compare the yield ratio of these decay modes between data and Monte Carlo. We test different track momentum regions for the kaons and pions in two-body and multi-body X_s final states separately, and calibrate the tracking efficiencies with 1.7 to 4.4% uncertainties. The kaon and pion veto efficiencies are checked with and without a veto for several inclusive modes. The kaon veto efficiency is checked with the same $\eta \to \pi^+\pi^-\pi^0$ data. The pion veto efficiency is checked with $\phi \to K^+K^-$ decays from an inclusive high momentum ϕ sample and

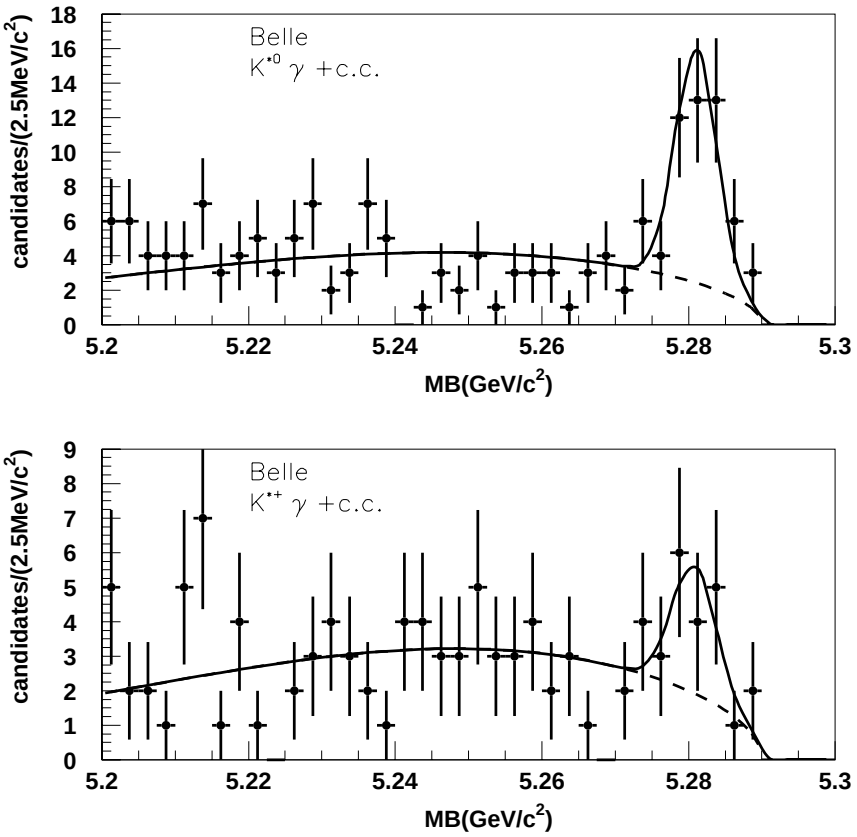

FIG. 4. The beam constrained mass (M_B) distributions for the $B^0 \to K^*(892)^0\gamma$ (top) and $B^+ \to K^*(892)^+\gamma$ (bottom) channels. The curve is the result of fitting with a signal Gaussian (solid line) on top of the background shape (dashed line) determined from the sideband analysis.

a $D_s^+ \to \phi\pi^+$ decay sample. The kaon and pion veto efficiency is calibrated with 0.8% and 0.7% uncertainties respectively. The π^0 and K_S^0 reconstruction efficiencies are tested with an inclusive D^{*+} decay sample where D^0 decays into $K^-\pi^+$, $K^-\pi^+\pi^0$ and $K_S^0\pi^+\pi^-$. We calibrate the π^0 and K_S^0 reconstruction efficiency with 7% and 9% uncertainties where the largest uncertainty comes from the D^0 branching fraction uncertainty in the PDG tables [18]. We use a sample of $B^- \to D^0\pi^-$ followed by $D^0 \to K^-\pi^+$ decays to calibrate the π^0/η veto and the SFW (inclusive analysis) or likelihood ratio (exclusive analysis) cut efficiencies. To test the likelihood ratio cut efficiency, we weighted the helicity angle distribution to follow the $\sin^2\theta_H$ distribution. We find the combined efficiencies are in agreement with 6% uncertainties.

In the inclusive analysis, the signal reconstruction efficiency is calibrated for 16 different modes separately. The correctly reconstructed fraction varies from 60 to 90% with at most 10 percent of cross-feeding between different modes. We obtain the M_{X_s} distribution shown in Fig. 7, which clearly highlights the $K^*(892)$ mass peak and is in good agreement with the model for higher resonances.

We take the uncertainty on extending our measurement into the full energy range by varying the Fermi momentum parameter of ref. [13], from 0.21 to 0.39 GeV/c in our recon-

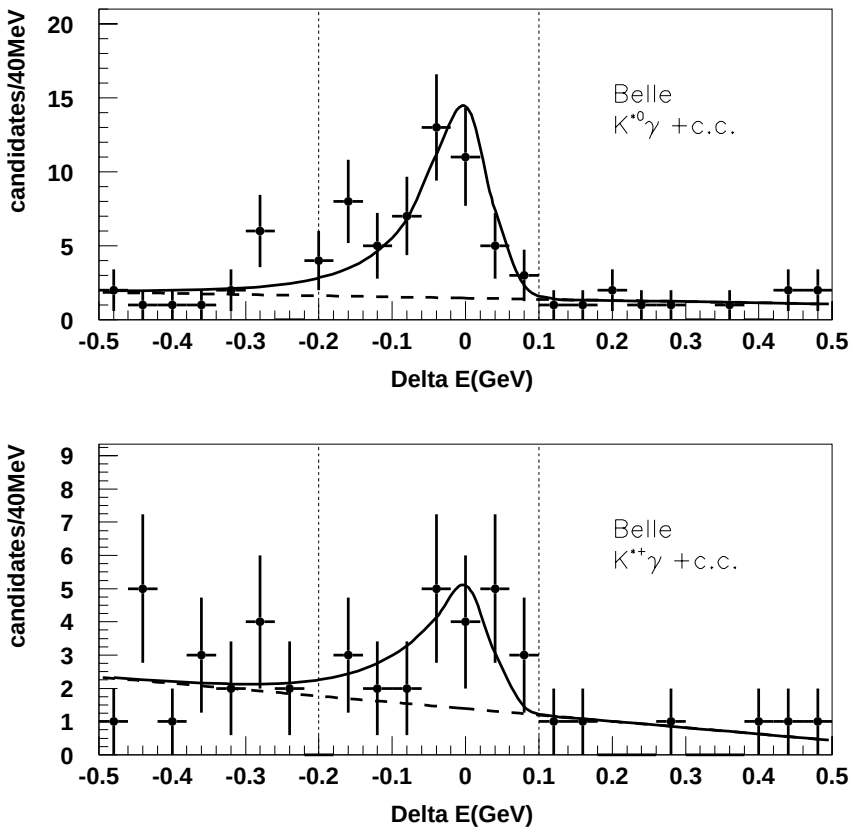

FIG. 5. The energy difference (ΔE) distributions for the $B^0 \to K^*(892)^0\gamma$ (top) and $B^+ \to K^*(892)^+\gamma$ (bottom) channels. The curve is the result of fitting the signal (solid line) on top of the expected background shape (dashed line). The dotted lines indicate the selected signal region.

struction efficiency estimation. The population in each individual final state varies at most by 10%. We then combine these numbers and quote the variation in the combined signal efficiency as the theoretical error.

Finally we obtain the $b \to s\gamma$ branching fraction as

$$\mathcal{B}(b \to s\gamma) = (3.34 \pm 0.50^{+0.34+0.26}_{-0.37-0.28}) \times 10^{-4}$$

where the first error is the statistical error, the second error is the systematic error of our measurement and the third error is the theoretical error. The dominant source of the statistical error comes from the background subtraction procedure. We also extract the branching fraction for the $E_\gamma > 2.1$ GeV range,

$$\mathcal{B}_{E_\gamma > 2.1\ \mathrm{GeV}}(b \to s\gamma) = (3.01 \pm 0.46^{+0.27+0.22}_{-0.31-0.24}) \times 10^{-4}$$

where the model dependent uncertainty is slightly reduced.

In the exclusive analysis, the resulting signal efficiencies are $(14.08 \pm 1.32)\%$ for $B^0 \to K^{*0}\gamma$ and $(7.07 \pm 0.81)\%$ for $B^+ \to K^{*+}\gamma$ channels. We obtain $38.3 \pm 7.2^{+2.0}_{-1.4}$ and $11.0 \pm 4.6^{+1.6}_{-0.8}$ event

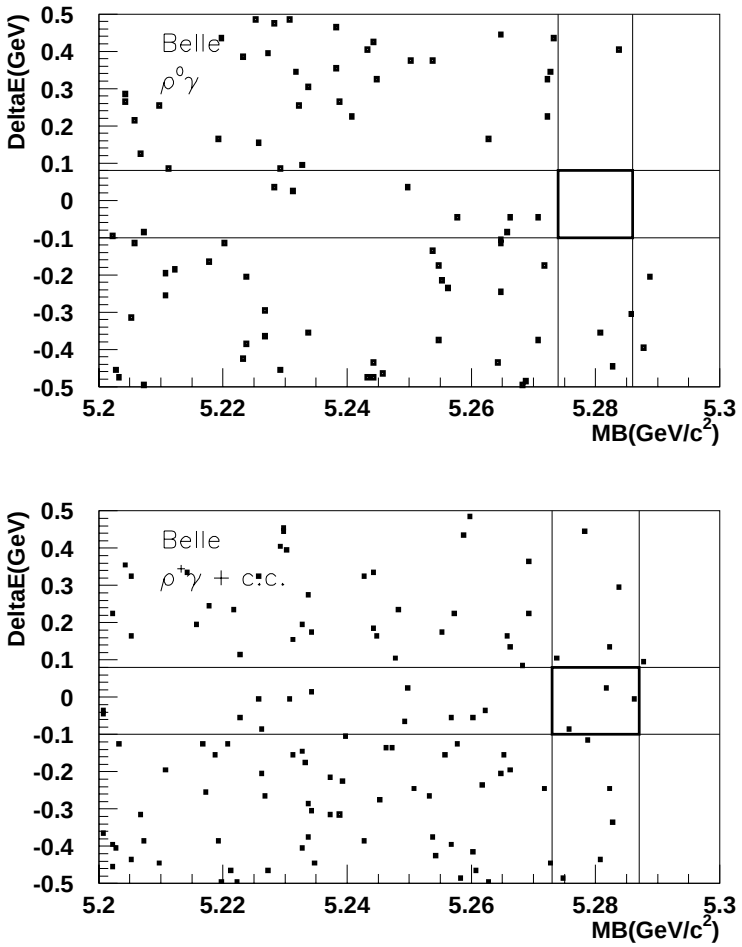

FIG. 6. The ΔE-M_B distributions for the $B^0 \to \rho(770)^0\gamma$ (top) and $B^+ \to \rho(770)^+\gamma$ (bottom) channels. We find 0 and 3 candidates in the respective signal regions.

yield respectively where the first and second errors are statistical and systematic errors in the fitting procedure. We obtain the exclusive branching fractions

$$\begin{aligned} \mathcal{B}(B^0 \to K^{*0}\gamma) &= (4.94 \pm 0.93^{+0.55}_{-0.52}) \times 10^{-5} \\ \mathcal{B}(B^+ \to K^{*+}\gamma) &= (2.87 \pm 1.20^{+0.55}_{-0.40}) \times 10^{-5}. \end{aligned}$$

where the first error is the statistical error, the second error is the systematic error.

For the $B \to \rho\gamma$ search, the signal efficiencies are $(6.8 \pm 0.7)\%$ for $B^0 \to \rho^0\gamma$ and $(5.8 \pm 0.7)\%$ for $B^+ \to \rho^+\gamma$ channels. We estimate 1.1 ± 0.4 and 1.8 ± 0.5 background events from the sideband data, where the sideband is defined as $-0.1 < \Delta E < 0.4$ GeV and $M_B > 5.2$ GeV/c^2 and outside of the signal region. The expected $K^*\gamma$ background is 0.08 events for $B^0 \to \rho^0\gamma$ and 0.25 events for $B^+ \to \rho^+\gamma$ searches. In the $\rho^0\gamma$ channel there are no candidates,

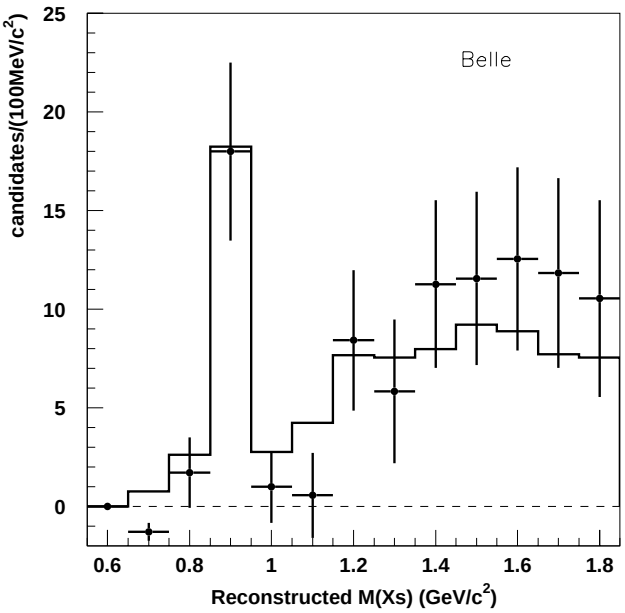

FIG. 7. The strange final state invariant mass (M_{X_s}) distribution after background subtraction (data points). The histogram shows the expected M_{X_s} distribution from the model of ref. [13].

and in the $\rho^+\gamma$ channel the excess is consistent with a background fluctuation. The upper limit of the signal yield is obtained using the method in [19] with the background expectation lowered by 1σ. We determine upper limits using efficiencies and $N_{B\bar{B}}$ lowered by 1σ:

$$\begin{aligned} \mathcal{B}(B^0 \to \rho^0\gamma) &< 0.56 \times 10^{-5} \quad (90\%\ \text{C.L.}) \\ \mathcal{B}(B^+ \to \rho^+\gamma) &< 2.27 \times 10^{-5} \quad (90\%\ \text{C.L.}). \end{aligned}$$

In order to set an upper limit on $\mathcal{B}(B\to\rho\gamma)/\mathcal{B}(B\to K^*\gamma)$, we performed the $K^*\gamma$ reconstruction using the same tight likelihood ratio cut to cancel out major systematic uncertainties. We obtained consistent $B\to K^*\gamma$ branching fractions and set an upper limit $\mathcal{B}(B^0\to\rho(770)^0\gamma)/\mathcal{B}(B\to K^*(892)^0\gamma) < 0.14$ (90% C.L.). Using the prescription $\mathcal{B}(B\to\rho\gamma) \equiv 2\mathcal{B}(B\to\rho(770)^0\gamma)$ in [21], we obtain

$$\mathcal{B}(B\to\rho\gamma)/\mathcal{B}(B\to K^*\gamma) < 0.28 \quad (90\%\ \text{C.L.}).$$

V. DISCUSSIONS

We have measured the inclusive and exclusive radiative B meson decay branching fractions into strange final states, and set uppper limits on $\mathcal{B}(B \to \rho\gamma)$.

The inclusive branching fraction is consistent with the Standard Model predictions, e.g. $(3.28 \pm 0.33) \times 10^{-4}$ in [1]. It is also consistent with the recent unpublished CLEO result $(3.15 \pm 0.35 \pm 0.32 \pm 0.26) \times 10^{-4}$ [20] and the ALEPH result $(3.11 \pm 0.80 \pm 0.72) \times 10^{-4}$ [3].

The exclusive branching fractions are both in agreement with the only existing result from CLEO, $\mathcal{B}(B^0 \to K^*(892)^0\gamma) = (4.55^{+0.72}_{-0.68} \pm 0.34) \times 10^{-5}$ and $\mathcal{B}(B^+ \to K^*(892)^+\gamma) = (3.76^{+0.89}_{-0.83} \pm 0.28) \times 10^{-5}$ [21]. The error of the exclusive analysis is dominated by statistics which we expect to quickly improve in coming runs.

The $B \to \rho\gamma$ search does not show a signal. We demonstrate that the Belle ACC provides essential separation from $K^*\gamma$. We extend the existing limit [21] with a smaller data sample. With the current data sample and an assumed branching fraction of 2.5×10^{-6} we expect to observe roughly one event. We therefore require a data set 10 times larger to observe a significant signal.

VI. ACKNOWLEDGEMENTS

We gratefully acknowledge the efforts of the KEKB group in providing us with excellent luminosity and running conditions and the help with our computing and network systems provided by members of the KEK computing research center. We thank the staffs of KEK and collaborating institutions for their contributions to this work, and acknowledge support from the Ministry of Education, Science, Sports and Culture of Japan and the Japan Society for the Promotion of Science; the Australian Research Council and the Australian Department of Industry, Science and Resources; the Department of Science and Technology of India; the BK21 program of the Ministry of Education of Korea and the Basic Science program of the Korea Science and Engineering Foundation; the Polish State Committee for Scientific Research under contract No.2P03B 17017; the Ministry of Science and Technology of Russian Federation; the National Science Council and the Ministry of Education of Taiwan; the Japan-Taiwan Cooperative Program of the Interchange Association; and the U.S. Department of Energy.

REFERENCES

[1] K. Chetyrkin, M. Misiak, M. Münz, Phys. Lett. **B400**, 206 (1997); Erratum ibid. **B425**, 414 (1998).

[2] M. Alam *et al.*, CLEO Collaboration, Phys. Rev. Lett. **74**, 2885 (1995).

[3] R. Barate *et al.*, ALEPH Collaboration, Phys. Lett. **B429**, 169 (1998).

[4] For example, F. Borzumati, C. Greub, Phys. Rev. **D58**, 074004 (1998); M. Ciuchini, G. Degrassi, P. Gambino, G. F. Giudice, Nucl. Phys. **B534**, 3 (1998); C. Bobeth, M. Misiak, J. Urban, Nucl. Phys. **B567** 153 (2000).

[5] A. Ali, H. Asatrian, C. Greub, Phys. Lett. **B429** 87 (1998).

[6] KEK accelerator group, KEKB B-Factory Design Report, KEK Report 95-7, 1995.

[7] Belle Collaboration, Technical Design Report, KEK Report 95-1, 1995.

[8] H. Hirano *et al.*, KEK Preprint 2000-2. submitted to Nucl. Instr. Meth. A; M. Akatsu *et al.*, DPNU-00-06, submitted to Nucl. Instr. Meth. A.

[9] G. Alimonti *et al.*, KEK preprint 2000-34.

[10] T. Iijima *et al.*, "Aerogel Cherenkov counter for the Belle detector", in the Proceedings of the 7th International Conference on Instrumentation for Colliding Beam Physics, Hamamatsu, Japan, Nov. 15–19, 1999.

[11] H. Kichimi *et al.*, submitted to Nucl. Instr. Meth. A.

[12] H. Ikeda et al., Nucl. Instr. Meth. **A441**, 401 (2000).

[13] A. Ali, C. Greub, Phys. Lett. **B259**, 182 (1991).

[14] A. L. Kagan, M. Neubert, Eur. Phys. J. **C7**, 5 (1999).

[15] T. Sjöstrand, Comp. Phys. Comm. **82**, 74 (1994).

[16] The virtual calorimeter and the fisher discriminant variables are used for example in D. M. Asner *et al.*, CLEO Collaboration, Phys. Rev. **D53**, 1039 (1996).

[17] G. Fox and S. Wolfram, Phys. Rev. Lett. **41**, 1581 (1978).

[18] Particle Data Group, R. M Barnett *et al.*, Phys. Rev. D **54**, 1 (1996).

[19] G. Feldman and R. Cousins, Phys. Rev. **D57**, 3873 (1998).

[20] S. Glenn *et al.*, CLEO Collaboration, contribution paper to the 29th International Conference on High Energy Physics, Vancouver, Canada, CLEO-CONF-98-17, 1998.

[21] T. Coan *et al.*, CLEO Collaboration, Phys. Rev. Lett. **84**, 5283 (2000).